Journal of Power Sources 229 (2013) 159–169

Contents lists available at SciVerse ScienceDirect

Journal of Power Sources

journal homepage: www.elsevier.com/locate/jpowsour

Model-based state of charge and peak power capability joint estimation of lithium-ion battery in plug-in hybrid electric vehicles

Rui Xiong [a,b], Hongwen He [a,*], Fengchun Sun [a], Xinlei Liu [a], Zhentong Liu [a]

[a] National Engineering Laboratory for Electric Vehicles, School of Mechanical Engineering, Beijing Institute of Technology, Beijing 100081, China
[b] DTE Power Electronics and Electric Drives Laboratory, University of Michigan-Dearborn, MI 48128, USA

HIGHLIGHTS

- A dynamic electrochemical polarization battery model is used for state estimation.
- An improved parameter identification test is used to get accurate model's parameters.
- The continuous peak power capability estimation approach is proposed.
- An AEKF-based SoC and peak power capability joint estimation approach is proposed.
- The robustness and reliability of the six steps joint estimator are evaluated.

ARTICLE INFO

Article history:
Received 8 November 2012
Received in revised form
28 November 2012
Accepted 1 December 2012
Available online 10 December 2012

Keywords:
Plug-in hybrid electric vehicles
Battery
Adaptive extended Kalman filter
State of charge
Peak power capability
Joint estimation

ABSTRACT

This paper uses an adaptive extended Kalman filter (AEKF)-based method to jointly estimate the State of Charge (SoC) and peak power capability of a lithium-ion battery in plug-in hybrid electric vehicles (PHEVs). First, to strengthen the links of the model's performance with battery's SoC, a dynamic electrochemical polarization battery model is employed for the state estimations. To get accurate parameters, we use four different charge–discharge current to improve the hybrid power pulse characteristic test. Second, the AEKF-based method is employed to achieve a robust SoC estimation. Third, due to the PHEVs require continuous peak power for acceleration, regenerative braking and gradient climbing, the continuous peak power capability estimation approach is proposed. And to improve its applicability, a general framework for six-step joint estimation approach for SoC and peak power capability is proposed. Lastly, a dynamic cycle test based on the urban dynamometer driving schedule is performed to evaluate the real-time performance and robustness of the joint estimation approach. The results show that the proposed approach can not only achieve an accurate SoC estimate and its estimation error is below 0.02 especially with big initial SoC error; but also gives reliable and robust peak power capability estimate.

1. Introduction

Energy crisis, environmental issues have promoted the development of various types of new energy vehicles, which has been listed as one of the seven strategic emerging industries in China [1,2]. Plug-in hybrid electric vehicles (PHEVs) are emerging as important personal transportation options for petroleum displacement and energy diversification, and its double operation modes, hybrid electric vehicle mode for suburbs or other driving cycles and pure electric vehicle mode for urban, is favorable; to meet these requirements, the battery system in PHEVs requires both high specific power and high energy [3–5].

The lithium-ion battery is widely used in many fields because of its advantages of high voltage, long cycle-life, high specific energy and high specific power, which also makes it a promising candidate for the PHEVs [6,7]. For PHEVs, on the one hand, battery State of Charge (SoC) is an important quantity, as it is a gauge of the remaining capacity in the battery. Thus, in order to manage the battery efficiently, an accurate SoC estimation method is one of the key issues. In addition, the accurate SoC estimation can improve the power distribution efficiency greatly, and also is the premise of the accurate estimates of the battery peak power capability [8–12]. On the other hand, accurate peak power estimates are critical in practical applications since it is necessary to

* Corresponding author. Tel./fax: +86 10 6891 4842.
E-mail address: hwhebit@bit.edu.cn (H. He).

0378-7753/$ – see front matter © 2012 Elsevier B.V. All rights reserved.
http://dx.doi.org/10.1016/j.jpowsour.2012.12.003

determine the power available in the moment to meet the acceleration, regenerative braking and gradient climbing power requirements without fear of over-charging or over-discharging the battery. More importantly, accurate peak power capability estimates for the battery will optimize the relation between the battery capacity and size with vehicle's performance, which benefits the vehicle's general potency [2,13,14]. Therefore, to provide an efficient guarantee for the optimization of PHEVs power systems, an accurate online SoC and peak power capability calculation algorithm is particularly critical to maintain optimum battery performance.

However, due to the strong time-variable and nonlinear performance of battery system, it is hard to measure its SoC directly for the various influence factors and complicated electrochemical process from the practice application. Some SoC estimation approaches which are presented with the development of battery powered electric vehicles can be generally classified into three kinds. The first is the direct measurement method, which involves measurements of voltage and electrochemical impedance [15,16]. However, due to the uncertain driving cycles, complex application environments, it is hard to measure the characterization parameters real-timely, and there is much to be solved for practical application. The second is ampere-hour counting method, which is based on both current measurement and integration [17]. However, its performance is highly dependent on the measuring accuracy of current, and this open-loop calculation method can easily lead to accumulated calculation errors due to uncertain disturbances from the practice application and lack of necessary corrective resolution. The third is the model-based method with filter algorithms, which carry out estimation by means of state-space battery models [18–24]. In Refs. [8–10], the authors use the extended Kalman filter (EKF) to adaptively estimate the SoC based on a simplified battery models. However, the Kalman filters-based algorithm strongly depends on the precision of the battery model and the predetermined variables of the system noise such as mean value, relevance and covariance matrix. An inappropriate information matrix of the system noise may lead to remarkable errors and divergence [12]. Therefore, an adaptive extended Kalman filter (AEKF)-based method has been applied to implement online SoC estimation in Refs. [12,23] to improve the estimate accuracy by adaptively updating the process and measurement noise covariance.

On the other hand, some peak power capability estimation approaches are presented with the development of electric vehicles technology [2,13,14]. The most commonly used approach is *hybrid pulse power characterization (HPPC) method* proposed by the Idaho National Engineering & Environmental Laboratory, which determines the static peak power in laboratory environments, and the estimates are over optimism. However, it is not suitable to estimate the continuous peak currents that are available for the next sampling interval Δt, additionally, the method neglects design limits like cell current, cell power or SoC [2]. As an improvement, the *voltage-limited* method was proposed by Plett [14]. However, these two *Rint* model-based methods can hardly simulate the dynamic voltage performance and the estimates will diverge from the practical capability. To solve this problem, the authors [13] propose a dynamic electrochemical polarization (EP) battery model-based multi-parameter peak power capability estimation method, and the experiment and simulation results show that the method has better performance than other commonly used methods. However, this method can efficiently estimate the peak power capability of the battery for the next sampling interval Δt, the estimates of multiple sampling intervals Δts can hardly be achieved, which is because the battery terminal voltage will change at any sampling interval when battery is discharged or charged at any current or power, therefore it is an inappropriate way to replace the sampling interval Δt with multiple sampling intervals Δts to get a longer time estimation. As a result, this method fails to provide continuous power for multiple sampling intervals, such as 15 s, 30 s, 60 s etc. when acceleration, regenerative braking or gradient climbing.

In this paper, based on the dynamic electrochemical polarization (EP) battery model, an AEKF-based SoC and peak power capability joint estimation approach for a 3.7 V/35 Ah $LiMn_2O_4$ lithium-ion battery used in PHEVs is proposed. A description of the EP battery model and its parameters identification process are given in Section 2. The six steps EP model-based SoC and peak power capability joint estimation approach with AEKF algorithm is depicted in Section 3. The experiment and evaluation for the proposed joint estimation approach is illustrated in Section 4. Finally, conclusions are drawn in Section 5.

2. Modeling the lithium-ion battery

2.1. The dynamic electrochemical-polarization battery model

To achieve a reliable battery state estimation, an accurate model must be built first. In Refs. [18,25], seven different battery models are introduced and evaluated. Due to the remarkable relaxation effect of the lithium-ion battery, we select dynamic electrochemical-polarization battery model, which uses an electrochemical battery model Nernst model to replace the open circuit voltage (OCV) part of the *Thevenin* model making SoC available as part of the model state and improving the model's accuracy. The schematic of the battery model is shown in Fig. 1. The electrical behavior of the proposed model can be expressed by Eq. (1).

$$\begin{cases} \dot{U}_p = -\dfrac{1}{C_p R_p} U_p + \dfrac{1}{C_p} I_L \\ U_t = U_{oc} - U_p - I_L R_o \end{cases} \tag{1}$$

where K_0, K_1, K_2, K_3 and K_4 are five constants chosen to make the model well fit the test data, R_o is the ohmic resistance and R_p is the polarization resistance. The polarization capacitance C_p is used to describe the transient dynamic voltage response during charging and discharging. U_p is the polarization voltage across C_p, U_t is the terminal voltage. Then the open circuit voltage U_{oc} can be described as follows:

$$U_{oc} = K_0 + K_1 \mathrm{SoC} + K_2/\mathrm{SoC} + K_3 \ln \mathrm{SoC} + K_4 \ln(1 - \mathrm{SoC}) \tag{2}$$

2.2. The parameters identification method

For battery equivalent circuit models, the commonly used parameters identification approach is multiple linear regression method with hybrid pulse power characterization data. To identify the parameters of the EP model, we need to identify the Nernst

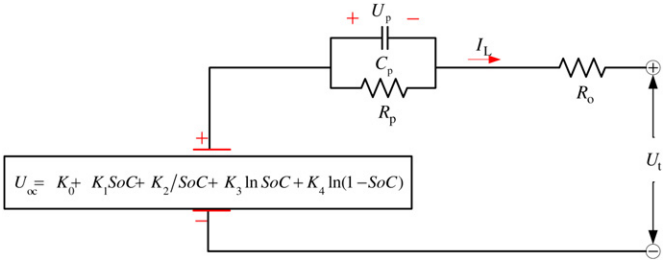

Fig. 1. The schematic diagram of the dynamic electrochemical-polarization model.

model's parameters firstly. The parameters of K_i ($i = 0, 1, 2, 3, 4$) can be calculated by linear fitting method with the experiment data of the OCV vs. the SoC. Then, to identify the other parameters, we firstly have a discretization process for dynamic nonlinear model and then we should build a regression equation for the discretization system. We use a regression equation [18] for the dynamic electrochemical-polarization model and is shown in Eq. (3).

$$\begin{cases} U_{t,k} = U_{oc} - R_o \times I_{L,k} - R_p \times I_{p,k} \\ I_{p,k} = \left(1 - \dfrac{\left(1 - \exp\left(\dfrac{-\Delta t}{\tau}\right)\right)}{\left(\dfrac{\Delta t}{\tau}\right)}\right) \times I_{L,k} + \left(\dfrac{\left(1 - \exp\left(\dfrac{-\Delta t}{\tau}\right)\right)}{\left(\dfrac{\Delta t}{\tau}\right)} - \exp\left(\dfrac{-\Delta t}{\tau}\right)\right) \times I_{L,k-1} + \exp\left(\dfrac{-\Delta t}{\tau}\right) \times I_{p,k-1} \end{cases} \quad (3)$$

where $I_{p,k}$ is the outflow current of C_p at the kth sampling time, $U_{t,k}$ is the terminal voltage at the kth sampling time, $I_{L,k}$ is load current at the kth sampling time respectively (assumed positive for discharge, negative for charge). The Δt is the sampling interval. The U_{oc} is determined by the SoC–OCV test. And the time constant of polarization ($\tau = R_p C_p$) required to be set in advance for regression operation, and for different time constant, different discriminant coefficients would be calculated; then an optimum time constant value will be achieved through finding the best discriminant coefficient by genetic algorithm [18].

2.3. Battery experiments

2.3.1. Test bench

The schematic of the built test bench is shown in Fig. 2, which consists of an Arbin battery test system BT2000 with MITS Pro soft for programming the BT2000, a thermal chamber for environment control and a host computer. The BT2000 can charge–discharge a battery according to the designed program with maximum voltage of 60 V and maximum charge/discharge current of 300 A with three scales (5 A/50 A/300 A), and its recorded data include current, voltage, temperature, charge–discharge Amp-hours (Ah) and Watt-hours (Wh) etc. The cell voltage also can be measured by the auxiliary channel, and its measuring range is 0–5 V. The measured data is transmitted to the host computer through TCP/IP ports. The errors of the Hall current and voltage sensors are less than 0.1%.

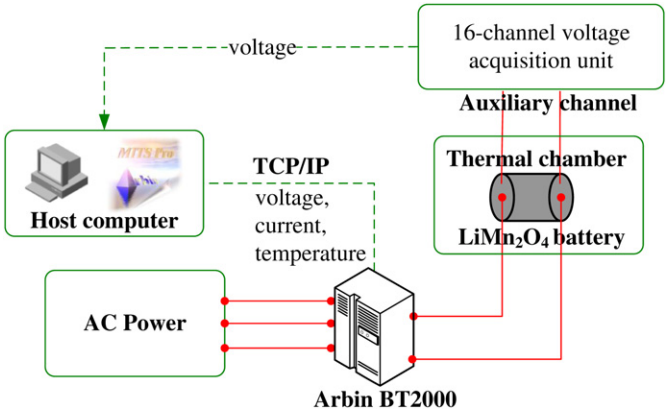

Fig. 2. The schematic of the battery test bench.

2.3.2. The specific hybrid pulse test

The battery is kept in the thermal chamber and the temperature is controlled within 30 ± 5 °C. Before the hybrid pulse test, the available capacity test, which is on the basis of the standard of Ref. [26], is performed to measure the battery's maximum available capacity. The maximum available capacity C_a of the battery is the number of ampere-hours that can be drawn from the battery at the standard current (C/3 rate), starting with the battery is fully charged, which maybe different with its nominal value due to the operation environment. For the fresh $LiMn_2O_4$ battery, the available capacity test shows that its actual maximum available capacity is 35.4 Ah, slightly higher than 35 Ah of the nominal capacity. Later, an OCV test is carried out to determine the SoC–OCV table.

Then, in order to acquire data to identify the model parameters, a specific hybrid pulse test procedure is conducted at 0.1 SoC intervals (constant current C/3 discharge segments) starting from 0.9 to 0.1 and each interval followed by a 1-h rest to allow the battery to get an electrochemical and thermal equilibrium condition before applying the next. The specific hybrid pulse test is similar with the traditional hybrid pulse power characterization test, but the specific hybrid pulse test uses four different charge–discharge currents to improve the applicability of the EP model under a more broad currents operation range of dynamic driving cycles. While the traditional hybrid pulse power characterization test only uses 1C (discharge) and 0.75C (charge) currents to build the model, and the model's parameters error will be arosed due to the battery's current-dependent relaxation effect and coulombic efficiency etc. Considering the battery current operation ranges of the battery used in PHEVs are always smaller than 3C, and the maximum current is less than 4C, we choose four currents (1C, 2C, 3C and 4C) to acquire identification data set. And the sampling interval in the paper is 1 s.

The specific hybrid pulse test results are shown in Fig. 3 including a sampling current curve in Fig. 3(a), a sampling voltage curve under SoC = 0.8 in Fig. 3(b), the current profiles in Fig. 3(c), the voltage profiles and the SoC profiles in Fig. 3(d).

2.3.3. The urban dynamometer driving schedule test

The urban dynamometer driving schedule (UDDS) is a standard time vs. velocity profile for urban driving vehicles and has been widely used in the evaluation of model accuracy and SoC estimate of battery management system [8–10,19,27]. For the driving-cycle testing of PHEVs batteries, we have calculated the required power from the powertrain operating with the UDDS cycle. Then the required power is reduced as a certain scale and then we use the power data to carry out the battery test. For the UDDS test, the battery SoC is controlled in the range of 0.15–0.9 according to the practical requirements of the electric vehicles. Due to the hard determination of the exact SoC value, herein we determine the initial SoC and the terminal SoC of the $LiMn_2O_4$ lithium-ion battery according to the definition of SoC with a standard charging

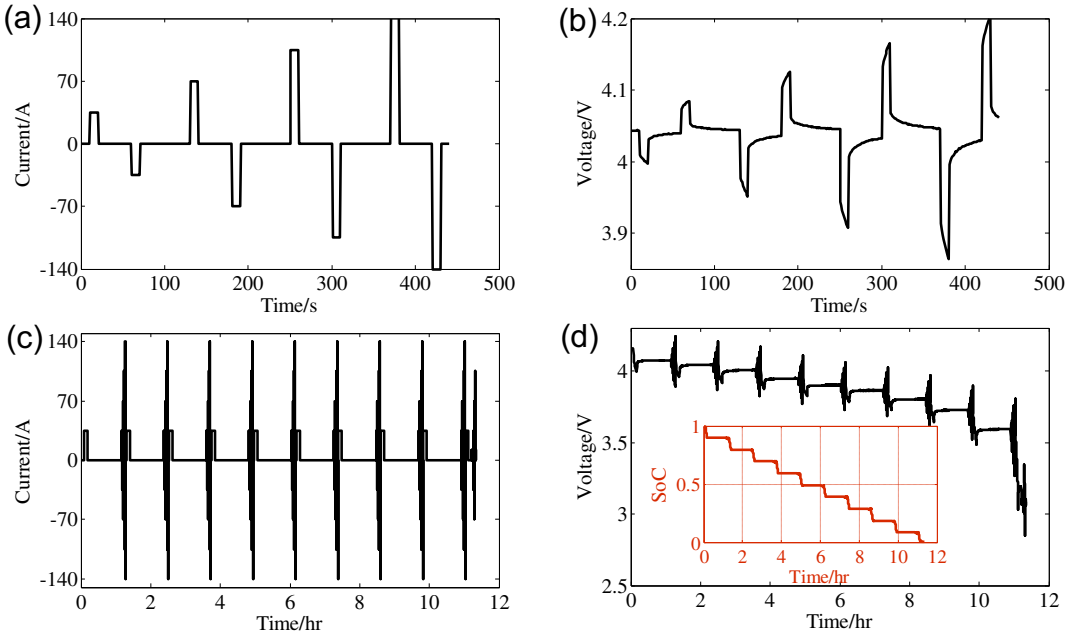

Fig. 3. The specific hybrid pulse test: (a) the sampling current vs. time profile of one cycle; (b) the sampling voltage vs. time profile of one cycle; (c) the current vs. time profiles; (d) the voltage vs. time profiles and the SoC vs. time profiles.

experiment and a further standard discharging experiment after finishing a test, so the initial SoC and the terminal SoC are accurate. The ampere-hour counting approach is used to calculate the SoC since it can keep track of the accurate SoC with an accurate initial SoC and a compensation of the coulombic efficiency. We also improve the SoC accuracy with a revision method based on the accurate terminal SoC. Considering all the battery experiments are carried out in a temperature chamber; the SoC calculation method is feasible with an acceptable accuracy. The eight consecutive UDDS test results are shown in Fig. 4 including the current profiles, voltage profiles and SoC profiles.

2.4. The parameters identification results of the model

The Nernst model's parameters identification results with the table of OCV vs. SoC are shown in Table 1 and the model's dynamic performance parameters results are shown in Table 2 with the specific hybrid pulse test.

3. SoC and peak power capability joint estimation approach

In order to use AEKF for the SoC and peak power capability joint estimation, we must first have a system model in a state-space form

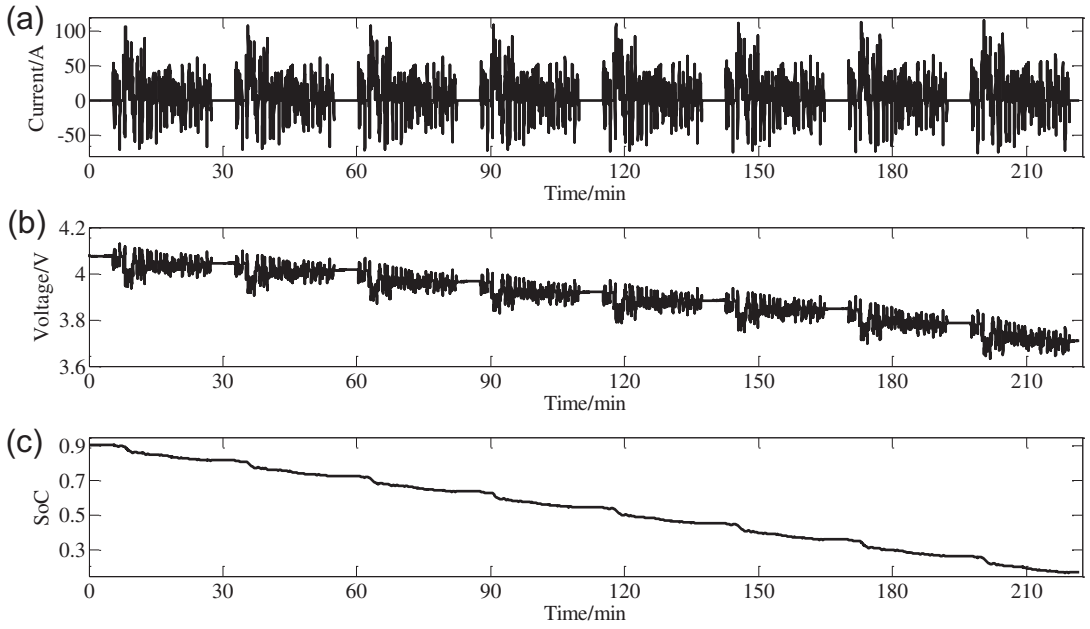

Fig. 4. The plots of the UDDS test: (a) the sampling current vs. time profiles; (b) the sampling voltage vs. time profiles; (c) the sampling SoC vs. time profiles.

Table 1
Identification results of Nernst model parameters.

K_0	K_1	K_2	K_3	K_4
3.8483	0.2441	−0.0124	0.0708	−0.0146

[23]. Specifically, we assume a very general framework for discrete-time lumped dynamic systems.

$$\mathbf{X}_{k+1} = \mathbf{A}\mathbf{X}_k + \mathbf{B}\mathbf{u}_k + \omega_k \tag{4}$$

$$\mathbf{Y}_{k+1} = \mathbf{C}\mathbf{X}_{k+1} + \mathbf{D}\mathbf{u}_k + \upsilon_k \tag{5}$$

We know that an AEKF-based approach will be used to estimate the battery SoC given noisy measurements [19,28,29]. To do so, we require a discrete state-space model similar with Eqs. (4) and (5) to describe the dynamics of the battery model. Transform Eq. (1) to a discrete system:

$$\begin{cases} U_{\mathrm{p},k+1} = U_{\mathrm{p},k}\exp\left(\dfrac{-\Delta t}{\tau}\right) + I_{\mathrm{L},k+1}R_{\mathrm{p}}\left(1-\exp\left(\dfrac{-\Delta t}{\tau}\right)\right) \\ U_{\mathrm{t},k+1} = U_{\mathrm{oc},k+1} - I_{\mathrm{L},k+1}R_{\mathrm{o}} - U_{\mathrm{p},k+1} \end{cases} \tag{8}$$

The state and observation function of the discrete system is as following:

$$\mathbf{X}_k = \begin{pmatrix} U_{\mathrm{p},k} \\ z_k \end{pmatrix},\ \mathbf{Y}_k = U_{\mathrm{t},k},\ \mathbf{u}_k = I_{\mathrm{L},k},\ \mathbf{A} = \begin{pmatrix} \exp\left(\dfrac{-\Delta t}{\tau}\right) & 0 \\ 0 & 1 \end{pmatrix},\ \mathbf{D} = [-R_{\mathrm{o}}]$$
$$\mathbf{B} = \begin{pmatrix} R_{\mathrm{p}}\left(1-\exp\left(\dfrac{-\Delta t}{\tau}\right)\right) \\ \dfrac{\eta_i \Delta t}{C_{\mathrm{a}}} \end{pmatrix},\ \mathbf{C} = \left.\frac{\partial U_{\mathrm{t}}}{\partial \mathbf{X}}\right|_{X=\widehat{X}_{k+1}^{-}} = \begin{bmatrix} -1 & \left.\dfrac{\mathrm{d}U_{\mathrm{oc}}(z)}{\mathrm{d}z}\right|_{z=z_{k+1}^{-}} \end{bmatrix} \tag{9}$$

where $\mathbf{X}_k$ is the system state vector at the kth sampling time, which represents the total effect of system inputs $\mathbf{u}_k$ on the present system operation, such as SoC. ω_k is the unmeasured "process noise" that affects the system state and υ_k is the measurement noise which does not affect the system state, but can be reflected in the system output estimates $\mathbf{Y}_k$. And ω_k is assumed to be Gaussian white noise with zero mean and covariance $\mathbf{Q}_k$; υ_k is assumed to be Gaussian white noise with zero mean and covariance $\mathbf{R}_k$. The matrices **A**, **B**, **C** and **D** describe the dynamics of the system, and are time varying and determined by looking up for the parameters table vs. SoC.

3.1. AEKF based SoC estimation approach

To carry out the SoC estimation process, According to the SoC definition, the battery SoC is the ratio of the remaining capacity to the available capacity:

$$z_k = z_0 - \int_0^k \eta_i I_{\mathrm{L},t}\mathrm{d}t/C_{\mathrm{a}} \tag{6}$$

where the SoC is denoted as z, z_k is the SoC at the kth sampling time, z_0 is the initial SoC, $I_{\mathrm{L,t}}$ is the instantaneous load current. The η_i is coulombic efficiency, which is the function of the current and the temperature and used for indicating the battery's capacity loss at different operating current. To describe the SoC with discrete form, then we can get equation:

$$z_k = z_{k-1} - \eta_i I_{\mathrm{L},k}\Delta t/C_{\mathrm{a}} \tag{7}$$

Table 2
Parameters identification results with SoC = 0.6, 0.7, 0.8.

SoC	C_{p}/F	R_{p}/mΩ	R_{o}/mΩ	τ/s
0.6	29,029	1.142	1.914	33.16
0.7	26,484	1.335	1.925	35.36
0.8	29,250	1.045	1.936	30.57

where $\mathrm{d}U_{\mathrm{oc}}(z)/\mathrm{d}z = K_1 - K_2/z^2 + K_3/z - K_4/(1-z)$ calculated from Eq. (2).

Then we can achieve AEKF-based SoC estimation on the basis of the implementation flowchart of the AEKF as listed in Fig. 5.

3.2. The EP dynamic model-based peak power capability estimation method

3.2.1. Instantaneous peak current estimation for single sampling interval

To build an EP model-based dynamic multi-parameter method for peak power capability estimation of lithium-ion battery, we must first have a discrete battery model written as follows on the basis of Eq. (8).

$$\begin{aligned} U_{\mathrm{t},k+1} = {} & U_{\mathrm{oc}}(z_{k+1}) - U_{\mathrm{p},k}\exp\left(\frac{-\Delta t}{\tau}\right) \\ & - I_{\mathrm{L},k+1}\left(R_{\mathrm{o}} + R_{\mathrm{p}}\left(1-\exp\left(\frac{-\Delta t}{\tau}\right)\right)\right) \end{aligned} \tag{10}$$

However, the peak currents cannot be solved directly from the maximum current $I_{\mathrm{L},k}$ since z_{k+1} itself is a function of the current $I_{\mathrm{L},k}$ and OCV is a nonlinear function of SoC [2]. To avoid this problem, the Taylor-series expansion is employed to linearize the equation and to solve the approximated values for the peak currents. The Taylor-series expansion equation for OCV is as follows:

$$\begin{aligned} U_{\mathrm{oc}}(z_{k+1}) &= U_{\mathrm{oc}}\left(z_k - I_{\mathrm{L},k+1}\frac{\eta_i \Delta t}{C_{\mathrm{a}}}\right) \\ &= U_{\mathrm{oc}}(z_k) - I_{\mathrm{L},k+1}\frac{\eta \Delta t}{C_{\mathrm{a}}}\left.\frac{\mathrm{d}U_{\mathrm{oc}}(z)}{\mathrm{d}z}\right|_{z=z_k} + R_1\left(z_k, I_{\mathrm{L},k+1}\frac{\eta_i \Delta t}{C_{\mathrm{a}}}\right) \end{aligned} \tag{11}$$

Considering the first-order residual $R_1(\cdot)$ being too small to affect the OCV at the next sampling time Δt, since the SoC's

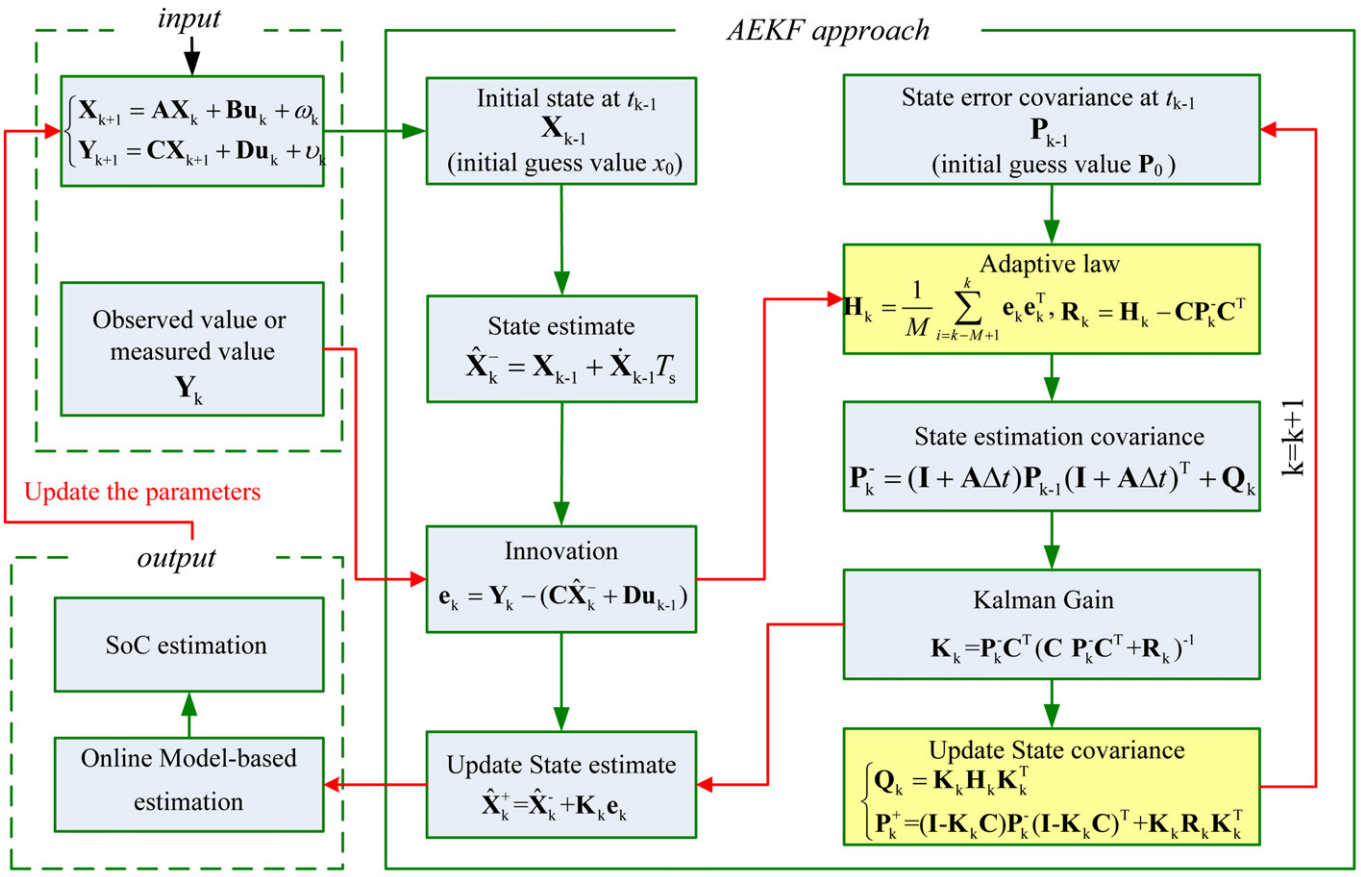

Note: $\mathbf{H}_k$ is the innovation covariance matrix based on the innovation sequence inside a moving estimation window of size M. $\mathbf{Q}_k$ and $\mathbf{R}_k$ for the $\mathbf{Q}$ and $\mathbf{R}$ at the kth sampling time respectively.Where $\mathbf{K}_k$is the kalman gain matrix; $\mathbf{e}_k$ is defined as the difference between the measurement and the observation $\mathbf{C}\hat{\mathbf{X}}_k^- + \mathbf{D}\mathbf{u}_{k-1}$, $\hat{\mathbf{X}}_k^+$ and $\hat{\mathbf{X}}_k^-$ are for the *priori* estimate *before* the measurement is taken into account and the *posteriori* estimate after the measurement is taken into account respectively.t_{k-1} is the initial time of calculation.

Fig. 5. An implementation flowchart of the AEKF algorithm.

variation per sampling time is very small [19,27], the $R_1(\cdot)$ can be viewed as $R_1(\cdot)\approx 0$. Then:

$$U_{t,k+1} = U_{oc}(z_k) - I_{L,k+1}\left(R_o + \frac{\eta\Delta t}{C_a}\left|\frac{dU_{oc}(z)}{dz}\right|_{z=z_k} + R_p\left(1-\exp\left(\frac{-\Delta t}{\tau}\right)\right)\right) - U_{p,k}\exp\left(\frac{-\Delta t}{\tau}\right) \quad (12)$$

Therefore, we can get the peak current estimates when takes the considerations of terminal voltage design limits – $U_{t,min}$ and $U_{t,max}$, and the computational equation is as follows:

$$\begin{cases} I_{max}^{dis,EP} = \dfrac{U_{oc}(z_k) - U_{p,k}\exp\left(-\frac{\Delta t}{\tau}\right) - U_{t,min}}{\frac{\eta_i\Delta t}{C_a}\left.\frac{dU_{oc}(z)}{dz}\right|_{z_k} + R_p\left(1-\exp\left(-\frac{\Delta t}{\tau}\right)\right) + R_o} \\ I_{min}^{chg,EP} = \dfrac{U_{oc}(z_k) - U_{p,k}\exp\left(-\frac{\Delta t}{\tau}\right) - U_{t,max}}{\frac{\eta_i\Delta t}{C_a}\left.\frac{dU_{oc}(z)}{dz}\right|_{z_k} + R_p\left(1-\exp\left(-\frac{\Delta t}{\tau}\right)\right) + R_o} \end{cases} \quad (13)$$

where $I_{min}^{chg,EP}$ and $I_{max}^{dis,EP}$ are the minimum charge currents and maximum discharge currents under the EP dynamic model-based method.

3.2.2. Continuance peak current estimation for multi sampling intervals

The peak current estimation approach calculated by Eq. (13) shows that the estimates have a big difference with different sampling interval Δt; and for electric vehicles application, we usually require to restrict the peak currents for some special conditions, such as acceleration, climbing, braking etc., for this respect, a continuance peak power estimation approach for multi sampling intervals, which is on the basis of the instantaneous peak current estimation approach for single sampling interval, is proposed here.

The input of the system is assumed constant between the kth sampling time t_k and the $(k+L)$th sampling time t_{k+L}, which is expressed by: $\mathbf{u}_{k+L}=\mathbf{u}_k$ with the sampling intervals is $L\times\Delta t$. Then, we can use the EP model to predict voltage at the $(k+L)$th sampling time into the future by:

$$\begin{cases} \mathbf{X}_{k+L} = \mathbf{A}\mathbf{X}_{k+L-1} + \mathbf{B}\mathbf{u}_{k+L-1} \\ \mathbf{Y}_{k+L} = \mathbf{C}\mathbf{X}_{k+L} + \mathbf{D}\mathbf{u}_{k+L-1} \end{cases} \quad (14)$$

Since Eq. (1) should be written in a linear discretization form as Eq. (14), therefore, for input constant over the entire prediction horizon (from time t_k to t_{k+L}), we have:

$$\mathbf{X}_{k+L} = \mathbf{A}^L\mathbf{X}_k + \left(\sum_{j=0}^{L-1}\mathbf{A}^{L-1-j}\mathbf{B}\right)\mathbf{u}_k \tag{15}$$

To find the minimum charging current $I_{\min,L}^{\mathrm{chg,EP}}$, the output of the system should satisfy the following equation:

$$U_{\mathrm{oc}}(z_{k+L}) - U_{\mathrm{p},k}\left(\exp\left(\frac{-\Delta t}{\tau}\right)\right)^L - I_{\min,L}^{\mathrm{chg,EP}}\left(R_{\mathrm{o}} + R_{\mathrm{p}}\left(1-\exp\left(\frac{-\Delta t}{\tau}\right)\right) \times\sum_{j=0}^{L-1}\left(\exp\left(\frac{-\Delta t}{\tau}\right)\right)^{L-1-j}\right) - U_{\mathrm{t,max}} = 0 \tag{16}$$

To find the maximum discharging current $I_{\max,L}^{\mathrm{dis,EP}}$, the output of the system should satisfy the following equation:

$$U_{\mathrm{oc}}(z_{k+L}) - U_{\mathrm{p},k}\left(\exp\left(\frac{-\Delta t}{\tau}\right)\right)^L - I_{\max,L}^{\mathrm{dis,EP}}\left(R_{\mathrm{o}} + R_{\mathrm{p}}\left(1-\exp\left(\frac{-\Delta t}{\tau}\right)\right) \times\sum_{j=0}^{L-1}\left(\exp\left(\frac{-\Delta t}{\tau}\right)\right)^{L-1-j}\right) - U_{\mathrm{t,min}} = 0 \tag{17}$$

Then, we can get the computational approach to predict peak current at the kth sampling time into the $(k+L)$th sampling time by:

$$\begin{cases} I_{\max,L}^{\mathrm{dis,EP}} = \dfrac{U_{\mathrm{oc}}(z_k) - U_{\mathrm{p},k}\left(\exp\left(\frac{-\Delta t}{\tau}\right)\right)^L - U_{\mathrm{t,min}}}{\frac{\eta_i L\Delta t}{C_{\mathrm{a}}}\left.\frac{\mathrm{d}U_{\mathrm{oc}}(z)}{\mathrm{d}z}\right|_{z_k} + R_{\mathrm{p}}\left(1-\exp\left(\frac{-\Delta t}{\tau}\right)\right)\sum_{j=0}^{L-1}\left(\exp\left(\frac{-\Delta t}{\tau}\right)\right)^{L-1-j} + R_{\mathrm{o}}} \\ I_{\min,L}^{\mathrm{chg,EP}} = \dfrac{U_{\mathrm{oc}}(z_k) - U_{\mathrm{p},k}\left(\exp\left(\frac{-\Delta t}{\tau}\right)\right)^L - U_{\mathrm{t,max}}}{\frac{\eta_i L\Delta t}{C_{\mathrm{a}}}\left.\frac{\mathrm{d}U_{\mathrm{oc}}(z)}{\mathrm{d}z}\right|_{z_k} + R_{\mathrm{p}}\left(1-\exp\left(\frac{-\Delta t}{\tau}\right)\right)\sum_{j=0}^{L-1}\left(\exp\left(\frac{-\Delta t}{\tau}\right)\right)^{L-1-j} + R_{\mathrm{o}}} \end{cases} \tag{18}$$

When the L is set as one, Eq. (18) is the same as Eq. (13).

3.2.3. Peak power capability estimation method

To make the battery's performance more safe and reasonable when the actual SoC is close to its design limits, we should control its discharge currents and maximize its charge currents when the actual SoC is close to its minimum design limits $z_{\min}$, otherwise, the battery will be over-discharged; on the other hand, we should control its charge currents and maximize its discharge currents when the actual SoC is close to its maximum design limits $z_{\max}$, otherwise, the battery will be over-charged. This is the key principle for the peak current estimation approach with the SoC-limited method, and computational equation and relevant description is shown as follows, which is derived from Eq. (7) when takes the consideration of SoC design limits.

$$\begin{cases} I_{\min,L}^{\mathrm{chg,soc}} = \dfrac{z_k - z_{\max}}{\eta_i L\Delta t/C_{\mathrm{a}}} \\ I_{\max,L}^{\mathrm{dis,soc}} = \dfrac{z_k - z_{\min}}{\eta_i L\Delta t/C_{\mathrm{a}}} \end{cases} \tag{19}$$

where $I_{\min,L}^{\mathrm{chg,SoC}}$ and $I_{\max,L}^{\mathrm{dis,SoC}}$ are the minimum charge current and maximum discharge current between the $L \times \Delta t$ sampling intervals under the SoC design limits. Once the current design limit is calculated, the peak currents with all limits enforced are calculated as:

$$\begin{cases} I_{\max}^{\mathrm{dis}} = \min\left(I_{\max}, I_{\max,L}^{\mathrm{dis,SoC}}, I_{\max,L}^{\mathrm{dis,EP}}\right) \\ I_{\min}^{\mathrm{chg}} = \max\left(I_{\min}, I_{\min,L}^{\mathrm{chg,SoC}}, I_{\min,L}^{\mathrm{chg,EP}}\right) \end{cases} \tag{20}$$

where $I_{\max}$ and $I_{\min}$ are design limits for the maximum discharge current and minimum charge current respectively. $I_{\min}^{\mathrm{chg}}$ and $I_{\max}^{\mathrm{dis}}$ are the minimum charge current and maximum discharge current respectively with all limits enforced. Then the peak power capability estimation based on the EP dynamic model-based can be calculated as follows:

$$\begin{cases} P_{\min}^{\mathrm{chg}} = \max\left(P_{\min}, U_{\mathrm{t},k+L}I_{\min}^{\mathrm{chg}}\right) \\ P_{\max}^{\mathrm{dis}} = \min\left(P_{\max}, U_{\mathrm{t},k+L}I_{\max}^{\mathrm{dis}}\right) \end{cases} \tag{21}$$

Then we can get the computational approach for peak power estimation when we take the terminal voltage calculation equation shown in Eq. (10).

$$\begin{cases} P_{\min}^{\mathrm{chg}} \approx \max\left(P_{\min}, \left(U_{\mathrm{oc}}(z_{k+L}) - U_{\mathrm{p},k}\left(\exp\left(\frac{-\Delta t}{\tau}\right)\right)^L - I_{\min}^{\mathrm{chg}}\left(R_{\mathrm{o}} + R_{\mathrm{p}}\left(1-\exp\left(\frac{-\Delta t}{\tau}\right)\right)\sum_{j=0}^{L-1}\left(\exp\left(\frac{-\Delta t}{\tau}\right)\right)^{L-1-j}\right)\right)I_{\min}^{\mathrm{chg}}\right) \\ P_{\max}^{\mathrm{dis}} \approx \min\left(P_{\max}, \left(U_{\mathrm{oc}}(z_{k+L}) - U_{\mathrm{p},k}\left(\exp\left(\frac{-\Delta t}{\tau}\right)\right)^L - I_{\max}^{\mathrm{dis}}\left(R_{\mathrm{o}} + R_{\mathrm{p}}\left(1-\exp\left(\frac{-\Delta t}{\tau}\right)\right)\sum_{j=0}^{L-1}\left(\exp\left(\frac{-\Delta t}{\tau}\right)\right)^{L-1-j}\right)\right)I_{\max}^{\mathrm{dis}}\right) \end{cases} \tag{22}$$

where P_{max}, P_{min} are the battery's power design limits, P_{max} denotes the peak discharge power and P_{min} denotes the peak charge power of its design limits respectively.

3.3. State of charge and peak power capability joint estimation algorithm

In order to use AEKF-based methods for the SoC and peak power capability joint estimation, we must first have a complete schematic of the online estimation and computational process. Therefore, a very general framework for online joint estimation, which named six steps joint estimation method, is shown in Fig. 6.The relevant processes are summarized as follows.

Step 1: *Initialization* – when given a random initial **X** matrix, we can get the model's parameters through looking up for the parameters tables and which is ready for AEKF-based online estimation approach. This initialization will be finished after the program code is loaded on the equipment.
Step 2: *Start* – when an input signals of the system, load current or required power is given, the charge–discharge current is loaded on the $LiMn_2O_4$ lithium-ion battery and the battery model simultaneously.
Step 3: *Correction and SoC estimation* – The terminal voltage error between the observer and the experimental data is adaptively reduced by updating the gain of the AEKF. And next the updated gain is used to compensate for the state estimation error. The SoC estimate is then fed back to update the parameters of the battery model for the SoC estimation at the next sampling time. And an accurate estimate for SoC and U_p will be reached quickly.
Step 4: *Dynamic peak current estimation* – Then, we require to calculate the peak currents with EP dynamic method and designed SoC-limited method, which will be performed by Eqs. (18) and (19).
Step 5: *Dynamic multi-parameter peak power capability estimation method* – When we take the consideration of the design limits of current, voltage and power, we can achieve the peak power estimates with Eqs. (20) and (22).
Step 6: *End* – Lastly, we can achieve the joint estimation for the SoC and peak power capability.

Table 3
Parameters limits for peak power capability estimation.

Parameters	Maximum value	Minimum value
SoC (z_{max}, z_{min})	0.9	0.15
U_t ($U_{t,max}$, $U_{t,min}$)/V	4.25	3.0
I_L (I_{max}, I_{min})/A	350	−175
P (P_{max}, P_{min})/W	1500	−750

4. Verification and discussion

This section will verify and evaluate the AEKF-based SoC and peak power capability joint estimation approach with different initial SoC under the UDDS test data. First, we should define the SoC design limits of the PHEVs batteries except for such design limits as voltage, power and current defined by the battery manufacturers. It is obvious that for different control strategies, the SoC limits maybe different. An example of parameter limits for peak power capability estimation is listed in Table 3.

Where the peak current and peak power design limits are restricted for continuous power, therefore for a short time which less than 60 s, the peak currents and powers will be much bigger than the values present in Table 3 and maybe 700/−350 A and 3000/−1500 W.

4.1. Verification for joint estimation method

The AEKF-based SoC estimation approach was conducted and the results are shown in Fig. 7 with the initial parameters as following:

$$x_0 = [4.1 \quad 0.9]^T,\ \mathbf{P}_0 = \begin{bmatrix} 1 & 0 \\ 0 & 1 \end{bmatrix},\ \mathbf{Q}_0 = \begin{bmatrix} 1 & 0 \\ 0 & 1 \end{bmatrix},\ R_0 = 1 \quad (23)$$

From Fig. 7(a), we can see the estimated terminal voltage tracks the experiment profiles well, and the details are shown in Fig. 7(b). From Fig. 7(b), it indicates that the terminal voltage error is less than 2% of its nominal voltage, which is because the AEKF-based algorithm can precisely estimate the voltage and timely adjust the Kalman gain matrix $\mathbf{K}_k$ according to the terminal voltage error between the measured data and the estimated values. From

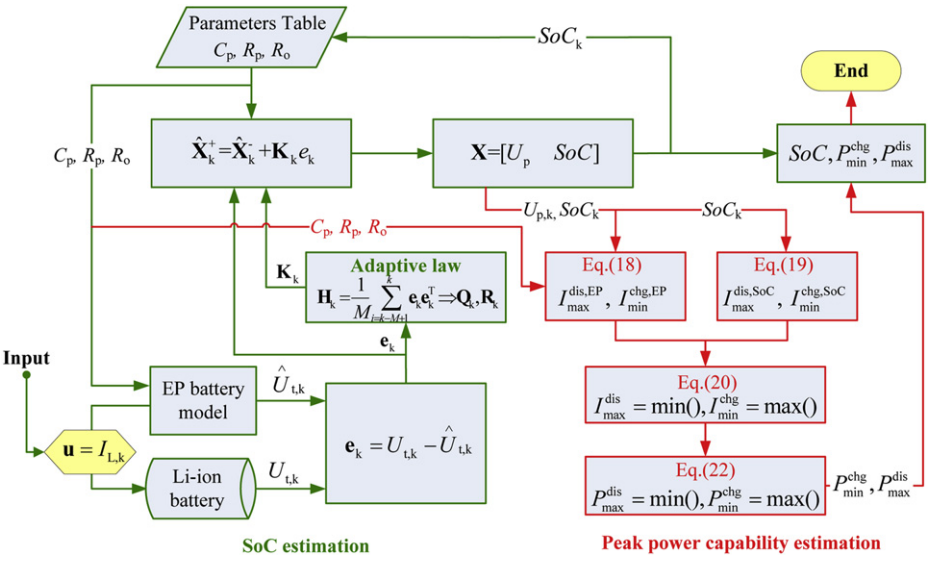

Fig. 6. The flowchart of the joint estimation under the AEKF-based adaptive observer.

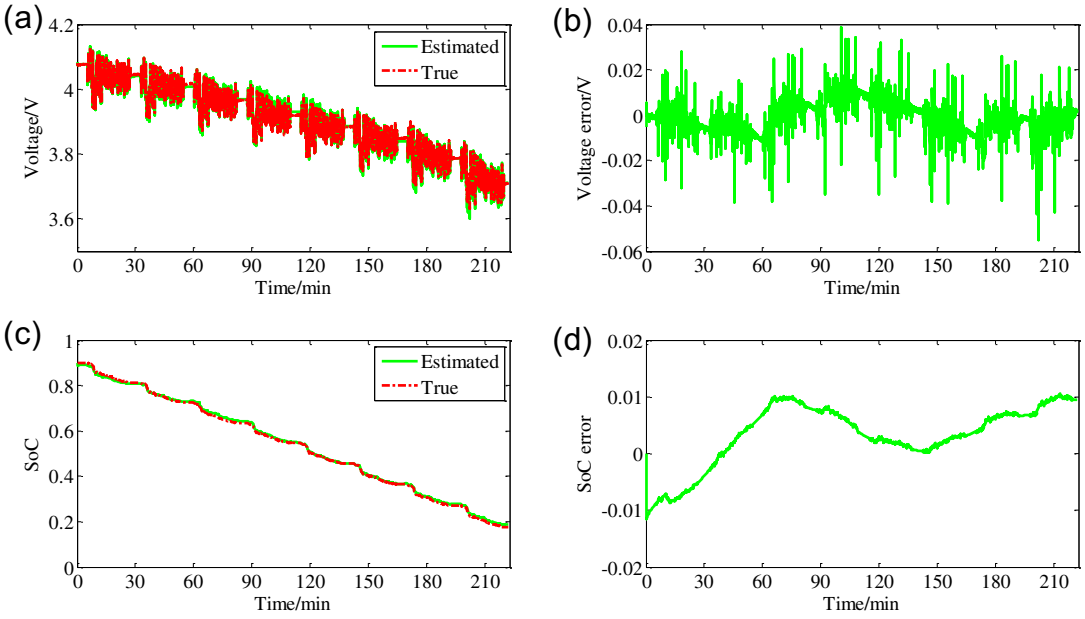

Fig. 7. AEKF-based SoC estimation results with an accurate initial SoC: (a) terminal voltage; (b) voltage estimation error; (c) SoC; (d) SoC estimation error.

Fig. 7(c), we can see the estimated SoCs track the true SoCs well, Fig. 7(d) shows that the range of the SoC estimation error is nearly between −0.01 and +0.01, which is quite accurate for SoC estimation.

And we also have calculated the real-time peak power capability with the six steps methods for 15 s 30 s and 60 s, the results are shown in Fig. 8.

From Fig. 8, we can see the more sampling intervals are required, the smaller of the absolute values of its peak currents and peak powers will be. Therefore, the instantaneous peak powers estimation are not suitable for longtime application or else the battery will be over-charged or over-discharged and damaged. Additionally, the EP model-based method can simulate the dynamic performance of the battery accurately and the dynamic power capability estimation results are well for practical use. However, the above estimation for SoC and peak power capability is based on an accurate initial SoC, and an accurate SoC estimation depends on two aspects according to the definition of SoC given by Eq. (6), one is the calculation of accumulated capacity consumption, another and most important is the robust performance for initial error of the SoC. The above results and analysis show that the SoC estimation error under the precise initial SoC is less than 0.02, which is quite desirable. In order to determine whether the joint estimation with AEKF approach can effectively solve the initial

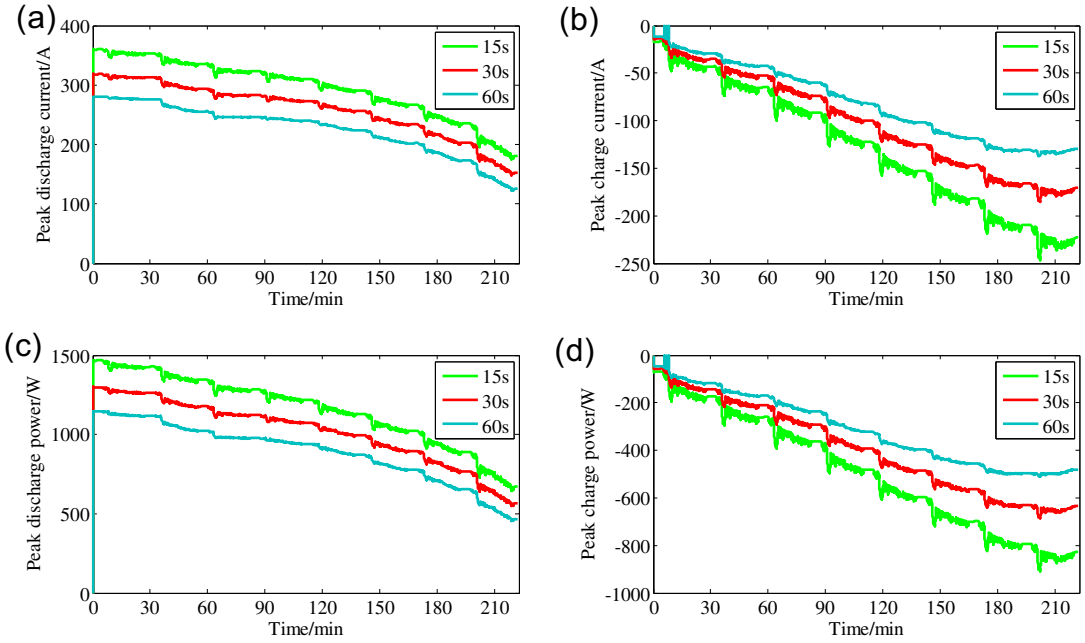

Fig. 8. AEKF-based peak power capability estimation results with accurate initial SoCs: (a) peak discharge current; (b) peak charge current; (c) peak discharge power; (d) peak charge power.

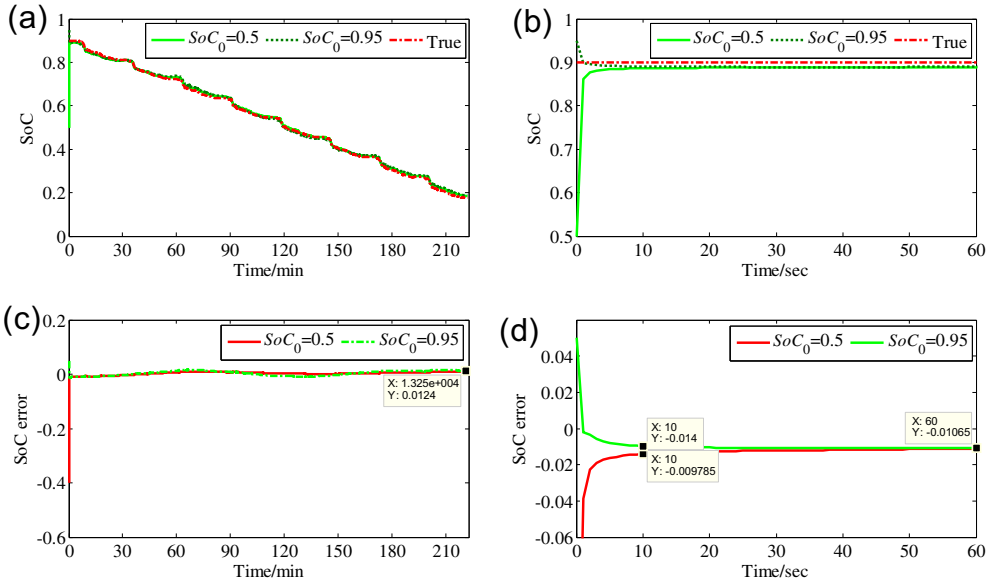

Fig. 9. Robust performance evaluation on SoC estimation results: (a) SoC estimation with $SoC_0 = 0.95$ and $SoC_0 = 0.50$; (b) zoom figure for (a); (c) SoC estimation error with $SoC_0 = 0.95$ and $SoC_0 = 0.50$; (d) zoom figure for (c).

error of the SoC, we carry out a further analysis for evaluating its robust performance.

4.2. Evaluation on the robustness of the joint estimation performance

Two different SoC initial values, 0.95 and 0.50, are preset and the corresponding SoC estimations are performed based on the UDDS cycles. The robust performance evaluation results for SoC are shown in Fig. 9.

From Fig. 9(a), we can see the SoC estimation results with the two different initial SoC are all almost the same as the true data, the zoom figure strengthens the description of the robustness performance of the AEKF-based SoC estimation approach. Fig. 9(b) indicates the proposed method ensure the robustness of SoC estimation after ten sampling intervals. To make the evaluation more clarity, we plot the SoC estimation error in Fig. 9(c) and (d), which indicates that the AEKF-based SoC estimation approach precisely estimates the SoC and timely modulates to adjust the Kalman gain matrix according to the terminal voltage error. And the SoC estimation error would be reduced to 0.02 after 10 sampling intervals, which is well suitable for PHEVs battery management system application. The precision of the SoC estimation ensures the reliable and robustness performance of the peak power capability estimation results. We use the peak discharge current estimates as an example to evaluate the robustness performance of the peak power estimation capability. Fig. 10 is the peak discharge currents estimation with different initial SoC values and the calculation sampling intervals is 30 s, the comparison profiles of the peak discharge current estimation results with three initial SoC values and the true SoC are plotted in Fig. 10(a), and zoom figure is in Fig. 10(b).

Due to the peak power capability estimation effect has a direct correction with the SoC estimation result from the calculation approach shown in Fig. 6, the accurate SoC estimation has been a strong guarantee for the robustness performance of the peak power capability estimation. Fig. 10(a) shows that the peak current estimates are almost the same for three SoC estimation results and the true SoC data, and the zoom figure shows that the estimation results can converge to the stable value within 10 sampling intervals especially with error initial SoC.

Therefore, the proposed AEKF-based joint estimation approach for SoC and peak power capability can efficiently estimate the SoC and peak power capability together accurately especially with big initial SoC error, and the maximum SoC estimation error is less than 2% after 10 sampling intervals. In addition, it is obvious that accurate SoC and available peak power capability estimates will benefit the Vehicle to Grid (V2G) application, and improve the control efficiency of the peak load regulation of the grid.

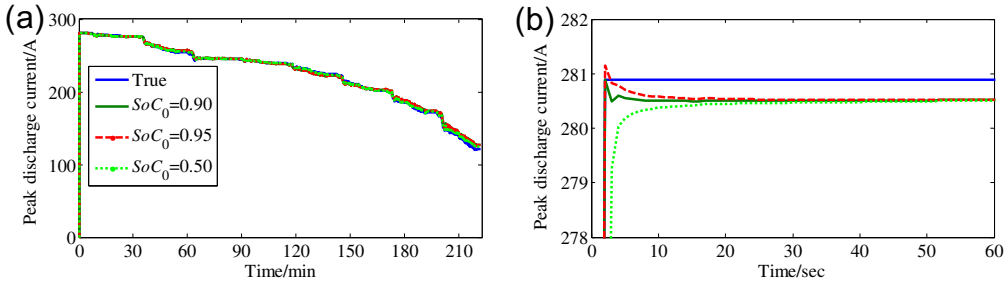

Fig. 10. Robust performance evaluation on peak power estimation results: (a) peak discharge current estimates of three initial SoC values and true value; (b) zoom figure for (a).

5. Conclusions

Based on the above analysis, the main concluding remarks can be made below:

(1) To model the dynamic performance of Lithium-ion battery accurately, the dynamic electrochemical polarization battery model is employed for state estimations; the model uses the Nernst model to build a relationship between the SoC and the open circuit voltage characteristic of the battery, therefore the model not only has the advantages of simulation accuracy for the terminal voltage, but also having a contribution to improve state estimation accuracy.
(2) To get accurate model's parameters and improve the dynamic performance simulation precision of battery model, we redefine the hybrid power pulse characteristic test with four different charge–discharge currents; and then we build a complete parameters identification process for the EP model.
(3) To achieve a robust SoC estimation, the AEKF approach is employed on the basis of the electrochemical polarization battery model.
(4) To achieve a continuous peak power requirement of the PHEVs, the continuous peak power capability estimation approach for multi-sampling intervals is proposed, and the corresponding peak current and peak power calculation methods are also built.
(5) An AEKF-based six-step joint estimation approach for SoC and peak power capability is proposed and its general operation flowchart is built. The simulation and experiment results indicate that the proposed approach not only has the advantages of online estimating the SoC accurately and robustly, and its peak error is less than 2% especially with big initial SoC error after 10 sampling intervals, but also can predict the peak power capability reliably and robustly.

The future work will focus on the joint estimation approach with the battery pack and online parameters identification method for the dynamic battery model, and the systematic validation test scheme for available peak power capability estimation.

Acknowledgments

This work was supported by the National High Technology Research and Development Program of China (2011AA112304, 2011AA11A228, 2011AA11A290) in part, the International Cooperation Research Program of Chinese Ministry of Science and Technology (2011DFB70020) in part, the Program for New Century Excellent Talents in University (NCET-11-0785) and also the Beijing Institute of Technology Post Graduate Students Innovation Foundation in part. The author would also like to thank the reviewers for their corrections and helpful suggestions.

References

[1] X. Li, J. Li, L. Xu, M. Ouyang, X. Han, L. Lu, C. Lin, J. Power Sources 195 (2010) 3338–3343.
[2] R. Xiong, H. He, F. Sun, K. Zhao, Energies 5 (2012) 1455–1469.
[3] R.F. Nelson, J. Power Sources 91 (2000) 2–26.
[4] S.J. Moura, D.S. Callaway, H.K. Fathy, J.L. Stein, J. Power Sources 195 (2010) 2979–2988.
[5] J. Belt, V. Utgikar, I. Bloom, J. Power Sources 196 (2011) 10213–10221.
[6] J. Kim, S. Lee, B.H. Cho, J. Power Sources 196 (2011) 2227–2240.
[7] H.S. Park, C.E. Kim, C.H. Kim, G.W. Moon, J.H. Lee, IEEE Trans. Ind. Electron. 56 (2009) 1464–1476.
[8] G.L. Plett, J. Power Sources 134 (2004) 252–261.
[9] G.L. Plett, J. Power Sources 134 (2004) 262–276.
[10] G.L. Plett, J. Power Sources 134 (2004) 277–292.
[11] H. He, X. Zhang, R. Xiong, Y. Xu, H. Guo, Energy 39 (2012) 310–318.
[12] H. He, R. Xiong, X. Zhang, F. Sun, J. Fan, IEEE Trans. Veh. Technol. 60 (2011) 1461–1469.
[13] F. Sun, R. Xiong, H. He, W. Li, J.E.E. Aussems, Appl. Energy 96 (2012) 3773–3785.
[14] G.L. Plett, IEEE Trans. Veh. Technol. 53 (2004) 1586–1593.
[15] F. Huet, J. Power Sources 70 (1998) 59–69.
[16] E.J. Dowgiallo Jr., US Patent 3984762, 1975.
[17] V.H. Johnson, J. Power Sources 110 (2002) 321–329.
[18] H. He, R. Xiong, J. Fan, Energies 4 (2011) 582–598.
[19] R. Xiong, H. He, F. Sun, et al., IEEE Trans. Veh. Technol. (2012). http://dx.doi.org/10.1109/TVT.2012.2222684.
[20] G.L. Plett, J. Power Sources 161 (2006) 1356–1368.
[21] G.L. Plett, J. Power Sources 161 (2006) 1369–1384.
[22] M. Charkhgard, M. Farrokhi, IEEE Trans. Veh. Technol. 57 (2010) 4178–4187.
[23] J. Han, D. Kim, M. Sunwoo, J. Power Sources 188 (2009) 606–612.
[24] M.A. Roscher, D.U. Sauer, J. Power Sources 196 (2011) 331–336.
[25] H. He, R. Xiong, H. Guo, S. Li, Energy Convers. Manage., http://dx.doi.org/10.1016/j.enconman.2012.04.014.
[26] Technical specification of battery management system for electric vehicles, Available at: www.catarc.org.cn/Upload/file/bzyj/PDF/zhengqiuyijian-sc27-19.pdf.
[27] Y. Chiang, W. Sean, J. Ke, J. Power Sources 196 (2011) 3921–3932.
[28] A.H. Mohamed, K.P. Schwarz, J. Geodesy 73 (1999) 193–203.
[29] G. Ye, P.P. Smith, J.A. Noble, Ultrasound Med. Biol. 36 (2010) 234–249.